Macromolecular Bioscience
www.mbs-journal.de

A Quantitative Description for Designing the Extrudability of Shear-Thinning Physical Hydrogels

*Hector Lopez Hernandez, Jason W. Souza, and Eric A. Appel**

Physically associated hydrogels (PHs) capable of reversible transitions between solid and liquid-like states have enabled novel strategies for 3D printing, therapeutic drug and cell delivery, and regenerative medicine. Among the many design criteria (e.g., viscoelasticity, cargo diffusivity, biocompatibility) for these applications, engineering PHs for extrudability is a necessary and critical design criterion for the successful application of these materials. As the development of many distinct PH material systems continues, a strategy to determine the extrudability of PHs a priori will be exceedingly useful for reducing costly and time-consuming trial-and-error experimentation. Here, a strategy to determine the property–function relationships for PHs in injectable drug delivery applications at clinically relevant flow rates is presented. This strategy—validated with two chemically and physically distinct PHs—reveals material design spaces in the form of Ashby-style plots that highlight acceptable, application-specific material properties. It is shown that the flow behavior of PHs does not obey a single shear-thinning power law and the implications for injectable drug delivery are discussed. This approach for generating design criteria has potential for streamlining the screening of PHs and their utility in applications with varying geometrical (i.e., needle diameter) and process (i.e., flow rate) constraints.

1. Introduction

Physically associated hydrogels (PH) are highly attractive materials for a broad range of applications ranging from 3D printing[1–7] to therapeutic cell delivery and controlled drug delivery.[8–11] Owing to their dynamic and noncovalent molecular structure, many PHs demonstrate complex, time-dependent viscoelastic and yield stress fluid behaviors. In general, they demonstrate elastically dominated, solid-like response near static conditions and facile, reversible transitions to viscously dominated, liquid-like responses upon the application of stress.[5,7,12–17] This seemingly paradoxical presentation of both rheological solid-like and liquid-like properties has been leveraged to enable the precise fabrication of 3D material scaffolds that effectively mimic the structural complexity of the extracellular matrix. They represent a significant portion of the tissue engineering scaffolds[18–25] and drug delivery platforms[8,10,26–29] developed over the past two decades because their ability to maintain a distinct 3D structure provides mechanical support for therapeutic cells in engineered tissues as well as localized retention of therapeutics with prolonged delivery kinetics. PHs have emerged as viable alternatives to postdelivery reaction strategies that rely on two-component postcure gelation, thermally induced gelation, or light-activated postcure polymerization by eliminating the need for initiators and external stimuli.

The crosslinking motifs in PHs are dynamic, noncovalent physical interactions. These interactions are diverse and span a variety of formulations, topologies, and chemistries, including host–guest interactions, hydrogen bonding, metal–ligand coordination, polymer–nanoparticle (NP) interactions, and protein–protein interactions.[12,27,30–33] Noncovalent crosslinks imbue PHs with highly complex rheological behaviors, including yielding, shear-thinning, viscoelastic, and thixotropic behaviors. PHs behave as solid-like gels when their physical interactions form a percolated crosslinked network. Their viscoelastic properties are impacted by both the thermodynamics and the dynamics of the physical interaction. The thermodynamics of the interaction control the proportion of bound crosslinks within the PH network. The interaction dynamics, however, dictate the rate of relaxation and reformation within the network, leading to solid-like viscoelasticity at time scales shorter than the relaxation time of the network and liquid-like viscoelasticity at longer time scales. Indeed, the dissociation rate of the physical crosslinking interactions in PHs has been shown to dictate the terminal relaxation time in unentangled physically crosslinked networks, while the association rate of the interaction dominates the recovery behavior of a disrupted network.[34–36]

Dr. H. Lopez Hernandez, J. W. Souza, Prof. E. A. Appel
Materials Science and Engineering
Stanford University
Stanford, CA 94305, USA
E-mail: eappel@stanford.edu
Prof. E. A. Appel
Department of Bioengineering
Stanford University
Stanford, CA 94305, USA
Prof. E. A. Appel
ChEM-H Institute
Stanford University
Stanford, CA 94305, USA
The ORCID identification number(s) for the author(s) of this article can be found under https://doi.org/10.1002/mabi.202000295.

DOI: 10.1002/mabi.202000295

 © 2020 Wiley-VCH GmbH

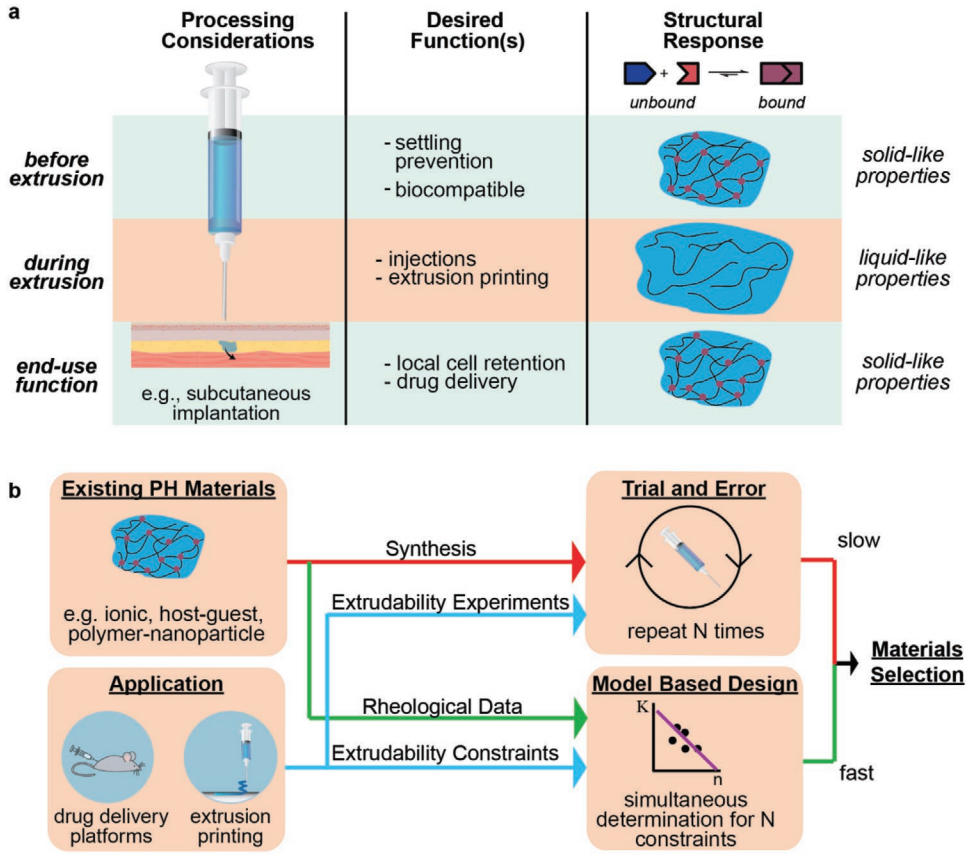

Figure 1. a) Material platforms for injectable drug delivery must meet several desired functions to successfully deliver cargo at the target site. Physically crosslinked hydrogels achieve this by responding to the stresses during extrusion by yielding and shear-thinning into a liquid-like material. The physical network then reforms as the dynamic crosslinks associate, creating a localized depot suitable for a variety of cargo delivery applications. b) Approaches for determining extrudability of PHs across applications. Model-based design offers clear benchmarks for extrudability, enabling rapid material selection without the need for trial-and-error experimentation.

Engineering PHs for applications in injectable drug delivery and 3D bioprinting remains a significant challenge. In general, PHs must be designed to meet the design constraints of three separate process domains: i) pre-extrusion, ii) extrusion, and iii) end-use (**Figure 1**a). When designing PHs, properties that affect end-use function are generally of primary importance (e.g., the stiffness of a 3D printed construct or the release kinetics of a drug delivery platform). Yet, optimization of end-use function often requires material design considerations which are opposed to those of extrudability (in 3D printing this is referred to as the printing window).[15,37]

For example, extending the duration of drug release from a depot formulation typically requires increasing the degree of crosslinking within the PH, thereby increasing viscosity sufficiently to preclude injectability. In 3D printing applications,[4,5,7,16] increasing the PH's yield stress may be desirable to improve the stability of printed objects, but it may also inadvertently increase the pressure required to print at comparable speeds.

There is an active area of research focused on tuning PH composition and structure to elicit a specific end-use function while retaining the ability for facile extrusion or injectability.[2,7,15] Here, we define both extrudability and injectability as functions of the pressure required to drive the flow of PHs through a channel. However, for therapeutic applications, we make the distinction that injectability is a comparison between the extrusion pressures required for clinical administration and the pressures that a human can comfortably generate. Extrudability is a more general term, encompassing the understanding of how the pressure required to drive fluid flow is a function of the process and geometrical parameters. There is a need for standardized and quantitative benchmarks by which to establish a PH as "extrudable" or "injectable" under application specific constraints. Unfortunately, many contributions to date simply demonstrate single PH extrusions through arbitrary needle gauges at arbitrary flow rates. Without a quantitative benchmark of extrudability, it is impossible to predict the relevance of PHs from the literature across a variety of other applications. Such a limitation is detrimental to further advancement of select PHs as the route of administration of therapeutic formulations can differ greatly (i.e., needle sizes, flow rates, catheters) for different indications. With the rapid advancement of novel PH chemistries and formulations,[25] it would be greatly advantageous to create strategies that allow for rapid determination of PH extrudability using rheological information without the need

© 2020 Wiley-VCH GmbH

for costly and time-intensive trial-and-error experimentation (Figure 1b).

In this contribution, we focused on developing quantitative property–function relationships by defining benchmark design criteria for the flow properties of extrudable PHs. In this manner, rheological characterization of a PH would readily reveal its extrudability for a range of application constraints, including needle geometries, flow rates, and extrusion pressures. Elucidation of target rheological properties a priori can enable design-based approaches that can accelerate materials discovery efforts.[38–40] This approach is a pillar in the engineering design method, which leverages mathematical models to define how variations in material properties will affect physical phenomena.[38,40,41] Herein, we validate a steady-state flow model for the extrusion of shear-thinning PHs to concretely establish design benchmarks in the form of Ashby-style plots. These plots reveal if a PH is extrudable for a specified set of geometrical (i.e., needle diameter) and process conditions (i.e., flow rate). These generalizable design constraints eliminate the need for extraneous trial-and-error experimentation. Critically, we emphasize that applications may impose shear rates above 3000 s^{-1} when using high gauge (small diameter) needles and highlight the need for collection of rheological data in application-relevant shear rate regimes to enable the use of effective design strategies.

2. Results and Discussion

In this work, we hypothesized that a steady-state flow model for the flow of a power law shear-thinning fluid—if valid for PHs—would enable improved materials design strategies. While flow models can be used for analysis or predictions of the extrusion pressure,[37,42–44] a flow model could be used inversely to identify the material properties that represent an extrudable PH. This approach unveils property–function relationships between the rheological properties and extrudability of PHs, which are applicable to any power-law shear-thinning PHs, regardless of chemistry and composition. Alginate-based hydrogels and polymer nanoparticle (PNP) hydrogels were used as model PHs because of their wide applicability, chemical versatility, and distinct crosslinking mechanisms. PNP hydrogels rely on multivalent, noncovalent interactions between polymers and the surfaces of adjacent nanoparticles to create dynamic crosslinks.[8,18,19,45–48] Alginate hydrogels form dynamic crosslinks through ionic interactions between divalent cations and carboxylate groups on alginate's guluronate residues and are the most commonly used biomaterial.[25,49–52] Additionally, most rheological data for PHs, regardless of their crosslinking mechanism, have demonstrated power-law shear-thinning behavior in shear flow.[30]

2.1. Flow Model

Modeling the flow of shear-thinning fluids is broadly used in processing applications in diverse fields to aid in process design. Likewise, modeling channel flow of PHs would enable the prediction of extrusion pressures from rheological data to aid in the design of PHs and extrusion processes using PHs. Many PHs exhibit both shear-thinning, whereby viscosity ($\eta = \sigma/\dot{\gamma}$) decreases as the shear rate or shear stress is increased, and yield stress behaviors.[53–56] Typically, a power law is used to describe the relationship between viscosity and shear rate where η is the viscosity, K is the consistency index, and n is the shear-thinning parameter (Equation (1)).[57]

$$\eta = K\dot{\gamma}^{n-1} \tag{1}$$

Using a power law to describe the shear rate dependence of the PH's viscosity, the momentum equation for steady-state pipe flow can be used to derive a relationship between the pressure required for extrusion and corresponding flow rate (Equation (2)).[58]

$$P = \left(\frac{3n+1}{n}\right)^n K\left(\frac{Q}{\pi}\right)^n \frac{2l}{R^{3n+1}} \tag{2}$$

The shear-thinning index (n) and consistency index (K) are material property parameters; tube radius (R) and length (l) are geometrical parameters; and pressure (P) and flow rate (Q) are process parameters. Importantly, this model assumes no-slip conditions at the wall of the cylinder, ideal power law behavior, no yield stress, negligible boundary effects, and steady-state conditions. We found the yield stress could be omitted from our modeling approach because the contribution of the yield stress to extrusion pressures is negligible under relevant geometrical and process constraints (Table S1, Supporting Information). Similarly, we found the contributions to the extrusion pressure from flow through the syringe and from the contraction between the syringe and needle are orders of magnitude lower than the contribution from flow through the needle (Figure S2, Supporting Information). These contributions were also omitted from our modeling approach.

2.2. Imposed Shear Rates for Injectable Drug Delivery and Extrusion-Based 3D Bioprinting

Alginate and PNP hydrogels are complex fluids, which demonstrate complex flow behaviors across a broad range of shear rates. It is important to clearly identify the stresses and shear rates relevant to extrusions and measure the rheological properties of the PHs within the same regime. The maximum shear stresses and rates in pipe flow occur at the wall of the pipe. The stress on the fluid at the wall (Equation (3)) is a function of the extrusion pressure (P_{ext}), radius (R), and length (l). The shear rate at the wall (Equation (4)) for a shear-thinning fluid is a function of the flow rate (Q), radius, and shear-thinning parameter (n), where $\frac{1}{n} = \frac{d\ln Q}{d\ln P}$ for a power law fluid.[57] It is important to recognize that given the applied pressure, the stress on the fluid (Equation (3)) is dependent only on the geometrical parameters and not the properties of the fluid. The shear rate (Equation (4)), however, is dependent on the shear-thinning properties of the fluid.

$$\sigma_{wall} = \frac{P_{ext}R}{2l} \tag{3}$$

© 2020 Wiley-VCH GmbH

$$\dot{\gamma}_{wall} = \frac{Q}{\pi R^3}\left(3 + \frac{d\ln Q}{d\ln P}\right) = \frac{Q}{\pi R^3}\left(3 + \frac{1}{n}\right) \quad (4)$$

Clearly, the stresses and shear rates imposed on the fluid during extrusion are dependent on the application and extrusion conditions, which can vary greatly across applications. Here we focus on translational, injectable drug delivery applications (e.g., oncology therapies, vaccinations, and diabetes treatments) that are preferred to intravenous administration because of shorter administration times and overall more comfortable patient experience.[59–61] Several oncology therapies (e.g., MabThera SC, Rituxan Hycela) are delivered at flow rates up to 2.3 mL min^{-1}, while there is interest in pursuing flow rates up to 18 mL min^{-1}.[62]

As an example scenario to probe the order of magnitude for the shear rates that dominate these clinically relevant flow rates in hypodermic needles, we consider a flow rate of 1 mL in 10 s (6 mL min^{-1}) and a clinically relevant 27 gauge needle (210 µm diameter). Assuming a shear-thinning parameter of 1 (Newtonian), the shear rate at the wall of the needle is ≈110 000 s^{-1}. For a 30 G needle (159 µm diameter), this shear rate is 253 000 s^{-1}. Additional shear rate calculations for various shear-thinning parameters, needle diameters, and flow rates are shown in Tables S2 and S3 (Supporting Information). These calculations are conservative, and the shear rate is greater for PHs with shear-thinning parameters less than 1. Nevertheless, these shear rates are three orders of magnitude greater than the typical shear rates reported for PHs. **Figure 2** demonstrates the broad range of shear rates for which an extrudable PH is exposed to, including those which are generally accessible within rotational rheometry limits, relevant to clinical injections, and important for 3D printing. Shear rates for 3D printing of biomaterials and bioprinting are estimates of the maximum shear rate possible at the published resolution to manufacturing times (Table S4, Supporting Information).[4] Though shear rates approaching 1000 s^{-1} may be rare today, the bioprinting field seeks to accelerate printing times and decrease the minimum feature size. One route to achieve this may be through the increase in extrusion flow rates and miniaturization of the printing needles. Predictions of the extrusion pressure for a given hydrogel in a prescribed extrusion configuration (i.e., needle length and diameter) rely on accurate materials parameters and it is necessary to measure the rheological behavior of PHs within the same range of shear rates that are relevant to their intended application.

2.3. Rheology of Alginate and Polymer-Nanoparticle Hydrogels

PNP hydrogels were formulated with 1 or 2 wt% of dodecyl-modified hydroxypropylmethylcellulose (HPMC-C_{12}) and 0 or 5 wt% poly(ethylene glycol)-*b*-poly(lactic acid) NPs, which are denoted as 1:0, 1:5, 2:0, and 2:5 (polymer wt%:NP wt%). Alginate formulations include 2 wt% alginate and 0, 5, 10, or 15 × 10^{-3} M calcium sulfate ($CaSO_4$), denoted as 0, 5, 10, and 15 × 10^{-3} M alginate formulations.

Both alginate and PNP hydrogels have been shown to demonstrate yielding and shear-thinning behavior above a threshold concentration of crosslinking moieties.[8,18,19,63] The addition of physical crosslinks between the polymer chains creates a structure which must yield before flow commences. For hydrogels that demonstrate yielding, there is a solid-like response below the apparent yield stress for which the material will not flow, and a transition to flow once the yield stress is surpassed.[56] Flow curves for PNP hydrogels are shown in **Figure 3**a and for alginate hydrogels in Figure 3b. Since these materials often possess a yield stress, measurements were collected with an imposed shear stress to capture preyield and yielding behavior as suggested by Barnes.[64] The stress sweep is followed by an imposed shear rate sweep from 1 to 100 s^{-1} to measure the flow behavior of the hydrogels. Figure 3ai,bi shows viscosity versus stress where the yielding phenomena is clearly observed as the viscosity drastically decreases by orders of magnitude for a small increase in stress. For PNP hydrogels (Figure 3ai, a sharp decrease in viscosity was observed between 10 and 20 Pa for the 1:5 formulation and 40–60 Pa for the 2:5 formulation. As expected for formulations without crosslinking and no structure to yield, continuous flow curves and no yield stress were observed for HPMC-C_{12} solutions (e.g., 1:0 and 2:0). For

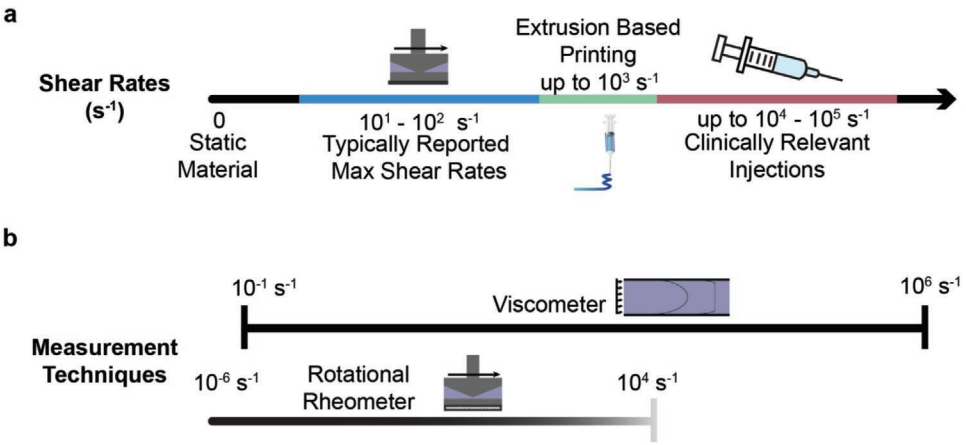

Figure 2. Possible shear rate limits for various processes and characterization techniques. Shear rates a) observed in injection/extrusion applications may exceed b) those readily measured with rotational rheometry.

© 2020 Wiley-VCH GmbH

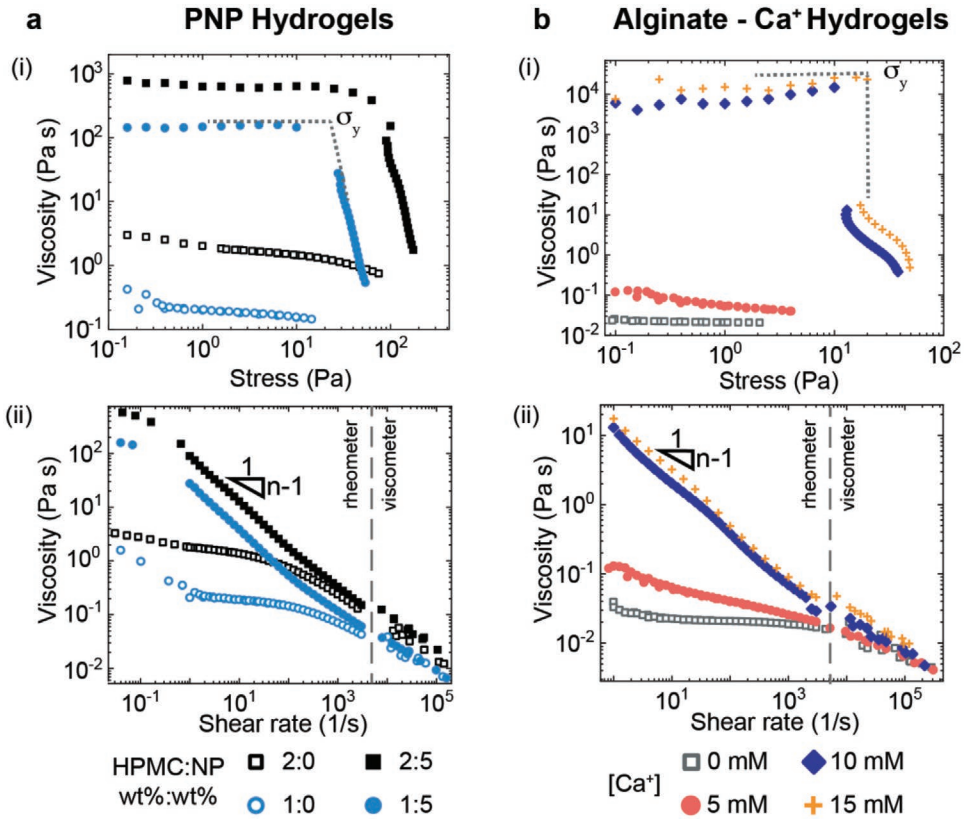

Figure 3. Rheology of physically associated a) polymer nanoparticle (PNP) hydrogels and b) alginate-Ca^{+} hydrogels. Rheological data for PNP and alginate hydrogels is plotted as i) viscosity versus stress to highlight the yield stress and transition to a flow regime and ii) viscosity versus shear rate showing drastic shear-thinning behavior. Data shown in (ii) was measured with a rotational rheometer up to a shear rate of 3000 s^{-1} and with a viscometer thereafter.

alginate hydrogels (Figure 3bi), a sharp decrease in viscosity was observed between 10 and 13 Pa for 10×10^{-3} M $CaSO_4$ and 17 and 20 Pa for 15×10^{-3} M $CaSO_4$. Formulations with 5×10^{-3} and 0 M $CaSO_4$ did not form hydrogels and no yield stress was observed. Small amplitude oscillatory shear measurements for these materials are shown in Figure S4 (Supporting Information).

As expected for PHs, the viscosity shown in Figure 3ii is shear-thinning for both PNP and alginate materials. Viscosity measurements were performed across five orders of magnitude to capture the behavior of the PHs at rest and under the conditions expected during extrusion through small diameter needles. Measurements were performed with a rotational rheometer up to a shear rate of 3000 s^{-1} and with a viscometer thereafter. Samples were ejected from the geometry in the rotational rheometer at shear rates above 3000 s^{-1}. As shown in Figure 2, a viscometer is often the recommended method for measuring a material's viscosity at high shear rates, eliminating the need for ad hoc corrections and the experimental challenges in a rotational rheometer.[57,65] Viscosity measurements were performed with 1 in., 27 gauge needles (210 µm diameter) at flow rates between 0.25 and 6 mL min^{-1}. The pressure and flow rate data for each extrusion were converted to the stress at the wall (Equation (3)) and shear rate at the wall (Equation (4)) to calculate the viscosity ($\eta(\dot{\gamma}_{wall}) = \frac{\sigma_{wall}}{\dot{\gamma}_{wall}}$). For Equation (4), $\frac{d \ln Q}{d \ln P}$ was calculated using a best fit polynomial to ln Q versus ln P, measured from the series of extrusions ($n > 5$). The derivative of the polynomial was calculated for each extrusion to approximate $\frac{d \ln Q}{d \ln P}$.

For both PNP and alginate hydrogels, the addition of crosslinking moieties increases the apparent viscosity dramatically at shear rates up to 100 s^{-1}. However, the difference between the viscosities of the polymer solution controls and the physically crosslinked hydrogels goes to zero as the shear rate is increased, where the viscosity of the crosslinked hydrogels approaches the viscosity of the non-crosslinked polymer solutions alone.

Material parameters n and K, shown in **Table 1**, were determined by fitting the flow portion (post yield) of viscosity versus shear rate data to a power law model (Equation (1)). The fits were performed in the low shear rate range 1–100 s^{-1} and in the high shear rate range between 10^3 and 10^5 s^{-1}. The low shear rate range is the most commonly reported for PHs, while the high shear rate range is the operative range for injectable drug delivery applications at clinically relevant flow rates. The shear-thinning parameter ranges from 0 to 1, where 1 corresponds to a Newtonian (shear rate independent) viscosity.

The power law response measured at high shear rates is significantly different than the power law response measured at shear rates in the range of 1–100 s^{-1}. The polymer solution

© 2020 Wiley-VCH GmbH

Table 1. Power law fits for alginate, HPMC-C_{12}, and respective hydrogels. 2 wt% alginate hydrogels with indicated Ca^{+} concentration ($\times 10^{-3}$ M). PNPs denoted as wt% HPMC-C_{12}: wt% NPs. *K* is the consistency index (Pa sn) and *n* is the shear-thinning parameter. Power law fits for shear rates in the range of 1–100 s^{-1} ($\dot{\gamma}_{low}$) and 4×10^3 to 200×10^3 s^{-1} ($\dot{\gamma}_{high}$).

		$\dot{\gamma}_{low}$		$\dot{\gamma}_{high}$	
		K [Pa s^n]	*N*	*K* [Pa s^n]	*n*
Alginate [$CaSO_4$] [$\times 10^{-3}$ M]	0	0.03	0.89	0.27	0.66
	5	0.12	0.74	0.24	0.69
	10	11.02	0.26	2.40	0.50
	15	16.09	0.29	7.88	0.42
PNPs polymer:NPs [wt%:wt%]	1:0	0.25	0.87	7.54	0.39
	1:5	27.37	0.15	5.96	0.44
	2:0	1.91	0.83	9.93	0.44
	2:5	91.03	0.15	60.03	0.31

controls were more shear-thinning in the high shear rate regime ($\dot{\gamma} > 1000$ s^{-1}) than in the low shear rate regime (1 $s^{-1} < \dot{\gamma} < 100$ s^{-1}). Gel-like formulations demonstrated extremely low shear-thinning parameters ($n < 0.3$) at low shear rates that increased significantly at higher shear rates from 0.15 to 0.31 for the 2:5 PNP hydrogels and from 0.29 to 0.42 for 15×10^{-3} M alginate hydrogels. We hypothesize that the increase in shear-thinning parameters at high shear rates is a consequence of further disrupting physical interactions within the hydrogels, resulting in a very broad yielding transition before simple power-law shear-thinning is observed. Relatively broad yielding transitions have been reported for polymers as the number of physical interactions increases, while sharp yielding transitions are observed for colloidal particle systems.[64,66]

2.4. Model Predictions of Extrusion Pressures

The flow model shown in Equation (2) was validated for shear-thinning hydrogels by comparing experimental measurements of extrusion pressures to model predictions using rheological data. Specifically, the assumption of ideal power law behavior at high shear rates relevant for injection or extrusion needed robust validation on account of the complex rheological behavior of PHs shown in the literature.[38,67–70]

Extrusion pressures were measured for both alginate and PNP hydrogel materials extruded through 1 in. long, 30 gauge ($R = 79.5$ µm) needles using a commercial syringe pump with an attached load cell. The forces required to drive fluid flow were measured with the load cell and converted to pressures by normalizing by the cross-sectional area of the syringe barrel ($P_{ext} = F/A_{syringe}$). Extrusion pressures were measured at flow rates in the range of 0.25 and 6 mL min^{-1} and are shown in Figure S6a (Supporting Information) for PNP hydrogels and Figure S6b (Supporting Information) for alginate hydrogels. Model predictions of the pressure for these extrusion conditions (geometry, flow rate) were made with Equation (2) using the material property parameters from rheology (*K*, *n*) (Table 1).

To highlight the importance of measuring the rheological behavior of PHs within the appropriate shear rate regime, model predictions were performed with fits to both the low and high shear rate regimes. **Figure 4**i compares the predicted extrusion pressures to the experimentally measured extrusion pressures (Figure S6, Supporting Information) using the power law fitting parameters from the low shear rate regime. With parameters from the low shear rate regime, the model fails to accurately predict the extrusion pressure for both alginate and PNP hydrogels. The model predictions overpredicted the extrusion pressures for HMPC-C_{12} and alginate solutions (i.e., no crosslinkers) and underpredicted the extrusion pressures of the PNP hydrogels and alginate hydrogels (i.e., with crosslinkers). Shear-thinning parameters of 0.15 observed in 1:5 and 2:5 hydrogels are significantly lower than those for typical polymer solutions and are likely a fingerprint of yielding since yielding events would be observed as a shear-thinning parameter of zero.[71]

Figure 4ii compares the predicted extrusion pressures to the experimentally measured extrusion pressures using the power law fitting parameters from the operative shear rates of the extrusion. The model provides greatly improved predictions of the extrusion pressure when using the appropriate rheological data (residuals shown in Figure S3, Supporting Information). Furthermore, the agreement between the model shown in Equation (2) and extrusions of PNPs and alginate hydrogels validates the use of a simple power-law shear-thinning model. This agreement suggests that the flow properties alone are a good first-order approximation for predicting the flow of a PH, despite their complex rheological behavior.

2.5. Modeling Extrudability for Materials Selection and Design

It is impossible to generally define a PH as extrudable without a precise definition of geometrical and process constraints. Using a validated flow model and complete flow curve, the extrusion pressure of a power-law shear-thinning PH can be predicted using Equation (2) for a given flow rate, pipe radius, and pipe length. Extrudability is then determined by comparing the calculated pressure to the allowable pressure in a given application (e.g., the pressure applicable by the average healthcare professional). This approach allows for determining the extrudability of PHs in arbitrary geometrical or process conditions (i.e., printhead, catheter, needle) without the need for costly trial-and-error experiments for each scenario.

Alternatively, a more comprehensive approach whereby a space of all acceptable viscosities for a variety of applications is possible. Instead of modeling one set of shear-thinning parameters for a PH to determine its extrudability, it is possible to define performance requirements (i.e., P_{max}, Q_{min}) to calculate a subset of shear-thinning parameters for a span of extrusion/injection geometries. This method is a pillar of the engineering design process where performance constraints are defined, and a range of material parameters is determined to facilitate material selection.[38,40] Often Ashby-style plots providing comparisons between material properties are used in the selection process to identify which materials possess the necessary combination of material parameters. For a power law fluid, it is possible

© 2020 Wiley-VCH GmbH

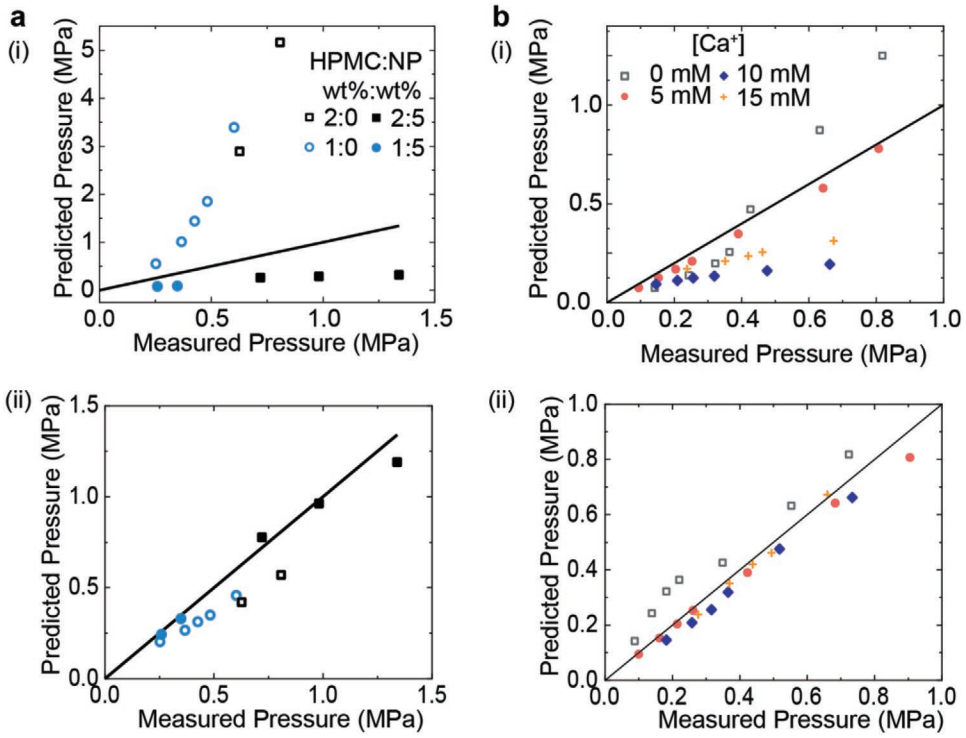

Figure 4. Flow predictions for a) PNP hydrogels and b) alginate hydrogels showing: i) predictions with material parameters from a power law fit to low shear rate data and ii) predictions with material parameters from a power law fit to shear rate data within the operative range. Experimental pressures from steady-state flow experiments, shown in Figure S6 (Supporting Information). Line with a slope of one is included to delineate a perfect prediction.

to write Equation (5) for the consistency index as a function of shear-thinning parameter to be used with Ashby-like plots to identify material parameter combinations of n and K that correspond to a truly "extrudable" PH.

$$K_{\max} \leq \left(\frac{P_{\max} R}{2 * L}\right)\left(\frac{\pi R^3}{Q_{\min}}\right)^n \left(\frac{n}{3n+1}\right)^n \quad (5)$$

In a simple example, we consider the applicability of alginate and PNP hydrogels in two injection scenarios using a 95 mm long, 1 mL syringe. The first scenario is subcutaneous injection using a 1 in. long, 27 gauge needle while the second scenario is catheter delivery via a 1 m long, 27 gauge catheter. We define injectability as the capability of reaching a flow rate of 1 mL per 10 s (6 mL min^{-1}) at a maximum pressure of 2.6 MPa. The maximum pressure ($P_{\max} = F_{\max}/\pi R_{\text{syr}}^2$) was determined by considering the force applicable by a person applying great effort, 50 N,[44,72] and the cross-sectional area of a 1 mL syringe with a diameter of 5 mm. **Figure 5**a is an Ashby-style plot of the consistency index versus the shear-thinning parameter where Equation (5) is shown for both scenarios. Equation (5) delineates a boundary below which are allowable shear-thinning parameters for which the injection pressure will not surpass the maximum applicable pressure. Using this analysis method, it becomes apparent that these formulations of alginate and PNP hydrogels are injectable at 6 mL min^{-1} through a 27 gauge, 1 in. long needle but are not injectable in a 27 gauge, 1 m long catheter.

For injectable drug delivery applications, especially those intended for patient use, it is important to consider relationship between the syringe selection and the maximum force applicable by a person.[44] The maximum pressure a person can apply depends heavily on the cross-sectional area on which force is applied. The maximum pressure generated by a person in a 1 mL (5 mm diameter) syringe is 2.6 MPa but the maximum pressure generated in a 5 mL (12 mm diameter) syringe is 442 kPa. This has a significant impact on the injectability of PHs in human driven injections. Equation (5) is plotted in Figure 5b for a flow rate of 6 mL min^{-1} in a 1 in. long, 30 gauge needle for both 1 and 5 mL syringes. Figure 5b shows the dramatic effects of syringe selection on injectability criteria, whereby these formulations are injectable using a 1 mL syringe but are not injectable using a 5 mL syringe. Beyond these examples, Equation (5) is incredibly useful for investigating the scaling relationship between geometrical and process constraints on acceptable material parameter combinations (Figure S7, Supporting Information). We envision that it will be a useful tool for designing future 3D printing processes and injectable drug delivery administration strategies to accommodate the diverse set of PHs.

2.6. Design Rules for Injectable Biomaterials

Designing an injectable biomaterial is typically constrained by many performance requirements which are often directly

© 2020 Wiley-VCH GmbH

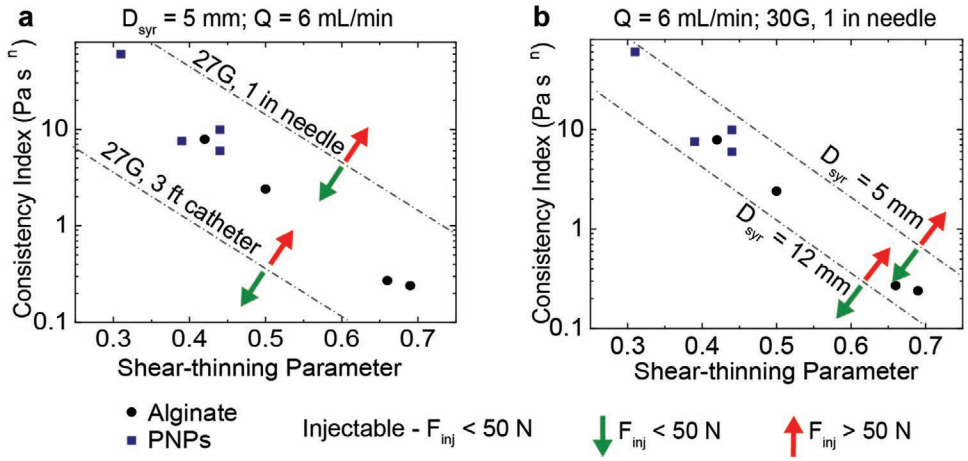

Figure 5. Ashby-style coplots for alginate and PNP hydrogels. Regions to the left of boundary lines are material property combinations representative on an injectable PH. a) Design boundary limits for a 1 mL syringe (D_{syr} = 5 mm) and 6 mL min^{-1} flow rate (Q). Alginate and PNPs are injectable in a 27 gauge, 1 in. needle but are not injectable in a 27 gauge, 3 ft catheter. b) Design boundary limits for a 30 gauge, 1 in. needle and flow rate of 6 mL min^{-1}. Alginate and PNPs are injectable using a 1 mL syringe but not a 5 mL syringe (D_{syr} = 12 mm).

opposing, as shown in Figure 1a. For example, both settling prevention and prolonged drug delivery benefit from a high viscosity while injectability necessarily requires a low viscosity. However, we highlight a key distinction where drug delivery and settling prevention depend on material properties in a static, nondeformed state and injectability depends on the viscosity at high shear rates in the range of 10^4–10^5 s^{-1}. We have shown with PNP and alginate hydrogels that the material response in each regime is indeed disparate across high and low shear rate regimes. The presence of an apparent yield stress for these PHs readily delineates solid and fluid regimes that are operative at different deformation amplitudes. For PNP hydrogels in flow, the low shear rate viscosity is increased by three orders of magnitude with the addition of 5 wt% NPs to HPMC-C_{12}. As the shear rate surpasses 10^3 s^{-1}, the viscosity for each polymer solution approaches the same magnitudes regardless of particle concentration. The same trend was discovered in alginate PHs where the apparent viscosity at lower shear rates increased by three orders of magnitude with the addition of $CaSO_4$ exceeding 10×10^{-3} M concentrations. At high shear rates, the sensitivity to $CaSO_4$ decreased dramatically. These observations highlight that it is possible to engineer materials exhibiting desirable material properties across distinct process regimes, whereby a hydrogel can be solid-like with a robust yield stress but maintain injectability provided the viscosity is sufficiently low at the injection-relevant shear rates. Efforts should focus on creating PHs with independently tuned rheological properties in the high and low shear rate regimes.

3. Summary and Conclusions

This work validates the applicability of a flow model for a power-law shear-thinning fluid and uses it to quantitatively define extrudability. Most importantly, it establishes a method for determining the extrudability of PHs from appropriate rheological data, eliminating the need for trial-and-error experimentation. It is shown that labeling something as "injectable" or "extrudable" requires a description of the intended geometrical configuration, applicable pressures, and intended flow rates in addition to the rheological properties of the PH. Ashby-style plots were used to condense this information into one plot to clearly demonstrate the extrudability of PHs across several scenarios. We validate our approach using two chemically and physically distinct PHs—including polymer-nanoparticle hydrogels and calcium-alginate hydrogels—and expect that other power-law shear-thinning PHs should obey the same property–function relationship regardless of chemical composition. The viscosity for both PHs exhibited drastic power-law shear-thinning at shear rates below 100 s^{-1} and a distinctly different and more moderate shear-thinning response at shear rates above 3000 s^{-1}. Given this observation, we emphasize the critical need for comprehensive rheological characterization of PHs in shear rate regimes that are pertinent to the applications of interest, which can exceed 3000 s^{-1}. These data are scarce in the literature and without them it is impossible to accurately model the extrudability of PHs at clinically relevant flow rates, making it impossible to determine their applicability across applications and precluding the engineering design process.

This contribution is a critical first step toward creating quantitative material benchmarks through property–function relationships for PHs. We have focused on modeling the extrudability of PHs but have not yet addressed the transition between extrusion and end-use function. Furthermore, while our approach demonstrated excellent predictive capabilities, we have assumed negligible effects of thixotropy, wall slip, extensibility, and syringe needle configurations different from those shown here. While our model will remain a good first-order approximation for the extrudability of most power-law shear-thinning PHs, consideration of these phenomena may be critical for some PHs.

© 2020 Wiley-VCH GmbH

Supporting Information

Supporting Information is available from the Wiley Online Library or from the author.

Acknowledgements

This research was financially supported by the Center for Human Systems Immunology with Bill & Melinda Gates Foundation (OPP1113682), the Bill & Melinda Gates Foundation (OPP1211043), the NIDDK (R01DK119254), and a Stanford Bio-X Interdisciplinary Initiatives Program Round 9 grant. H.L.H. was also partially supported by the NSF AGEP postdoctoral fellowship. J.W.S. was supported by the Stanford Ignite Summer Fellowship program and the NSF RET Teaching Engineering Design & Innovation EEC 1760810.

Conflict of Interest

The authors declare no conflict of interest.

Keywords

3D printing, biomaterials, hydrogels, rheology, shear-thinning

Received: August 21, 2020
Revised: October 19, 2020
Published online:

[1] M. Guvendiren, J. Molde, R. M. D. Soares, J. Kohn, *ACS Biomater. Sci. Eng.* **2016**, *2*, 1679.
[2] T. Jungst, W. Smolan, K. Schacht, T. Scheibel, J. Groll, *Chem. Rev.* **2016**, *116*, 1496.
[3] W. Jia, P. S. Gungor-Ozkerim, Y. S. Zhang, K. Yue, K. Zhu, W. Liu, Q. Pi, B. Byambaa, M. R. Dokmeci, S. R. Shin, A. Khademhosseini, *Biomaterials* **2016**, *106*, 58.
[4] M. E. Prendergast, J. A. Burdick, *Adv. Mater.* **2020**, *32*, 1902516.
[5] C. B. Highley, C. B. Rodell, J. A. Burdick, *Adv. Mater.* **2015**, *27*, 5075.
[6] M. Guvendiren, H. D. Lu, J. A. Burdick, *Soft Matter* **2012**, *8*, 260.
[7] D. Chimene, R. Kaunas, A. K. Gaharwar, *Adv. Mater.* **2020**, *32*, 1902026.
[8] E. A. Appel, M. W. Tibbitt, M. J. Webber, B. A. Mattix, O. Veiseh, R. Langer, *Nat. Commun.* **2015**, *6*, 6295.
[9] L. Zou, A. S. Braegelman, M. J. Webber, *ACS Appl. Mater. Interfaces* **2019**, *11*, 5695.
[10] D.-Q. Wu, T. Wang, B. Lu, X.-D. Xu, S.-X. Cheng, X.-J. Jiang, X.-Z. Zhang, R.-X. Zhuo, *Langmuir* **2008**, *24*, 10306.
[11] M. H. Chen, J. J. Chung, J. E. Mealy, S. Zaman, E. C. Li, M. F. Arisi, P. Atluri, J. A. Burdick, *Macromol. Biosci.* **2019**, *19*, 1800248.
[12] J. Malda, J. Visser, F. P. Melchels, T. Jüngst, W. E. Hennink, W. J. A. Dhert, J. Groll, D. W. Hutmacher, *Adv. Mater.* **2013**, *25*, 5011.
[13] M. H. Chen, L. L. Wang, J. J. Chung, Y.-H. Kim, P. Atluri, J. A. Burdick, *ACS Biomater. Sci. Eng.* **2017**, *3*, 3146.
[14] H. Wang, S. C. Heilshorn, *Adv. Mater.* **2015**, *27*, 3717.
[15] R. Levato, T. Jungst, R. G. Scheuring, T. Blunk, J. Groll, J. Malda, *Adv. Mater.* **2020**, *32*, 1906423.
[16] C. S. O'Bryan, T. Bhattacharjee, S. L. Marshall, W. G. Sawyer, T. E. Angelini, *Bioprinting* **2018**, *11*, e00037.
[17] B. D. Olsen, J. A. Kornfield, D. A. Tirrell, *Macromolecules* **2010**, *43*, 9094.
[18] A. K. Grosskopf, G. A. Roth, A. A. A. Smith, E. C. Gale, H. L. Hernandez, E. A. Appel, *Bioeng. Transl. Med.* **2020**, *5*, 1.
[19] H. L. Hernandez, A. K. Grosskopf, L. M. Stapleton, G. Agmon, E. A. Appel, *Macromol. Biosci.* **2019**, *19*, 1800275.
[20] B. A. Aguado, W. Mulyasasmita, J. Su, K. J. Lampe, S. C. Heilshorn, *Tissue Eng., Part A* **2012**, *18*, 806.
[21] L. Cai, R. E. Dewi, S. C. Heilshorn, *Adv. Funct. Mater.* **2015**, *25*, 1344.
[22] B. V. Slaughter, S. S. Khurshid, O. Z. Fisher, A. Khademhosseini, N. A. Peppas, *Adv. Mater.* **2009**, *21*, 3307.
[23] G. D. Nicodemus, S. J. Bryant, *Tissue Eng., Part B* **2008**, *14*, 149.
[24] X. Tong, F. Yang, *Adv. Healthcare Mater.* **2018**, *7*, 1701065.
[25] W. L. Ng, C. K. Chua, Y.-F. Shen, *Prog. Polym. Sci.* **2019**, *97*, 101145.
[26] Y. Dong, W. Wang, O. Veiseh, E. A. Appel, K. Xue, M. J. Webber, B. C. Tang, X. Yang, G. C. Weir, R. Langer, D. G. Anderson, *Langmuir* **2016**, *32*, 8743.
[27] S. Uman, A. Dhand, J. A. Burdick, *J. Appl. Polym. Sci.* **2020**, *137*, 48668.
[28] J. E. Mealy, J. J. Chung, H. H. Jeong, D. Issadore, D. Lee, P. Atluri, J. A. Burdick, *Adv. Mater.* **2018**, *30*, 1705912.
[29] Q. V. Nguyen, D. P. Huynh, J. H. Park, D. S. Lee, *Eur. Polym. J.* **2015**, *72*, 602.
[30] J. L. Mann, A. C. Yu, G. Agmon, E. A. Appel, *Biomater. Sci.* **2018**, *6*, 10.
[31] M. J. Webber, E. A. Appel, E. W. Meijer, R. Langer, *Nat. Mater.* **2016**, *15*, 13.
[32] L. Voorhaar, R. Hoogenboom, *Chem. Soc. Rev.* **2016**, *45*, 4013.
[33] F. M. Fumasi, N. Stephanopoulos, J. L. Holloway, *J. Appl. Polym. Sci.* **2020**, *137*, 49058.
[34] C. J. Dimitriou, G. H. McKinley, *Soft Matter* **2014**, *10*, 6619.
[35] K. E. Feldman, M. J. Kade, E. W. Meijer, C. J. Hawker, E. J. Kramer, *Macromolecules* **2009**, *42*, 9072.
[36] Z. Zhang, Q. Chen, R. H. Colby, *Soft Matter* **2018**, *14*, 2961.
[37] N. Paxton, W. Smolan, T. Böck, F. Melchels, J. Groll, T. Jungst, *Biofabrication* **2017**, *9*.
[38] A. Z. Nelson, K. S. Schweizer, B. M. Rauzan, R. G. Nuzzo, J. Vermant, R. H. Ewoldt, *Curr. Opin. Solid State Mater. Sci.* **2019**, *23*, 100758.
[39] B. M. Rauzan, A. Z. Nelson, S. E. Lehman, R. H. Ewoldt, R. G. Nuzzo, *Adv. Funct. Mater.* **2018**, *28*, 1707032.
[40] A. Z. Nelson, R. H. Ewoldt, *Soft Matter* **2017**, *13*, 7578.
[41] G. B. Olson, *Science* **2000**, *288*, 993.
[42] A. Allmendinger, S. Fischer, J. Huwyler, H.-C. Mahler, E. Schwarb, I. E. Zarraga, R. Mueller, *Eur. J. Pharm. Biopharm.* **2014**, *87*, 318.
[43] A. Allmendinger, R. Mueller, E. Schwarb, M. Chipperfield, J. Huwyler, H.-C. Mahler, S. Fischer, *Pharm. Res.* **2015**, *32*, 2229.
[44] T. E. Robinson, E. A. B. Hughes, A. Bose, E. A. Cornish, J. Y. Teo, N. M. Eisenstein, L. M. Grover, S. C. Cox, *Adv. Healthcare Mater.* **2020**, *9*, 1901521.
[45] L. M. Stapleton, A. N. Steele, H. Wang, H. L. Hernandez, A. C. Yu, M. J. Paulsen, A. A. A. Smith, G. A. Roth, A. D. Thakore, H. J. Lucian, K. P. Totherow, S. W. Baker, Y. Tada, J. M. Farry, A. Eskandari, C. E. Hironaka, K. J. Jaatinen, K. M. Williams, H. Bergamasco, C. Marschel, B. Chadwick, F. Grady, M. Ma, E. A. Appel, Y. J. Woo, *Nat. Biomed. Eng.* **2019**, *3*, 611.
[46] E. A. Appel, M. W. Tibbitt, J. M. Greer, O. S. Fenton, K. Kreuels, D. G. Anderson, R. Langer, *ACS Macro Lett.* **2015**, *4*, 848.
[47] E. A. Guzzi, G. Bovone, M. W. Tibbitt, *Small* **2019**, *15*, 1905421.
[48] O. S. Fenton, M. W. Tibbitt, E. A. Appel, S. Jhunjhunwala, M. J. Webber, R. Langer, *Biomacromolecules* **2019**, *20*, 4430.
[49] J. L. Drury, D. J. Mooney, *Biomaterials* **2003**, *24*, 4337.
[50] K. Y. Lee, D. J. Mooney, *Prog. Polym. Sci.* **2012**, *37*, 106.
[51] E. A. Silva, D. J. Mooney, *J. Thromb. Haemostasis* **2007**, *5*, 590.
[52] S. J. Bidarra, C. C. Barrias, P. L. Granja, *Acta Biomater.* **2014**, *10*, 1646.
[53] A. B. Metzner, J. C. Reed, *AIChE J.* **1955**, *1*, 434.

© 2020 Wiley-VCH GmbH

[54] A. B. Metzner, *Ind. Eng. Chem.* **1957**, *49*, 1429.
[55] B. O. A. Hedstrm, *Ind. Eng. Chem.* **1952**, *44*, 651.
[56] E. C. Bingham, *Bull. Bur. Stand.* **1916**, *13*, 309.
[57] C. W. Macosko, *Rheometry: Principles, Measurements, and Applications*, Wiley-VCH, New York **1994**.
[58] R. A. Chilton, R. Stainsby, *J. Hydraul. Eng.* **1998**, *124*, 522.
[59] X. Pivot, J. Gligorov, V. Müller, G. Curigliano, A. Knoop, S. Verma, V. Jenkins, N. Scotto, S. Osborne, L. Fallowfield, L. Fallowfield, V. Jenkins, J. Kilkerr, C. Langridge, K. Monson, E. H. Jakobsen, M. H. Nielsen, S. Linnet, A. Knoop, X. Pivot, H. Bonnefoi, M. Mousseau, L. Zelek, H. Bourgeois, C. P. Lefeuvre, T. Bachelot, T. Petit, E. Brain, C. Levy, J. Gligorov, D. Augustin, H. Graf, G. Heinrich, H. Kroening, S. Kuemmel, V. Müller, F. Overkamp, T.-W. Park-Simon, M. Schmidt, L. Perlova-Griff, C. Wolf, M. Colleoni, A. Ballestrero, A. Bernardo, A. S. Ribecco, L. Gianni, G. Curigliano, E. Brewczynska, J. Jassem, V. Shirinkin, A. Manikhas, V. Dvornichenko, M. Lichinitser, V. Semiglazov, G. Mukhametshina, I. Bulavina, E. E. Arranz, F. C. Ocon, G. L. Vivanco, J. S. Bofill, I. P. Quintela, A. S. Muñoz, Y. F. Pérez, J. C. Espinosa, J. V. Alvarez, R. L. del Prado, L. C. De Merino, J. M. P. García, S. E. Frances, P. Edlund, B. Norberg, A.-K. Wennstig, P. Lind, N. Hauser, C. Tausch, C. Camci, F. Arpaci, H. Abali, R. Uslu, S. Tahir, D. Wheatley, S. Chan, P. Barrett-Lee, K. McAdam, R. Simcock, R. Burcombe, R. El-Maraghi, N. Califaretti, S. Spadafora, S. Sehdev, A. Sami, S. Verma, *Ann. Oncol.* **2014**, *25*, 1979.
[60] X. Pivot, J. Gligorov, V. Müller, P. Barrett-Lee, S. Verma, A. Knoop, G. Curigliano, V. Semiglazov, G. López-Vivanco, V. Jenkins, N. Scotto, S. Osborne, L. Fallowfield, *Lancet Oncol.* **2013**, *14*, 962.
[61] I. Usach, R. Martinez, T. Festini, J.-E. Peris, *Adv. Ther.* **2019**, *36*, 2986.
[62] F. Schwarzenbach, C. Berteau, O. Filipe-Santos, T. Wang, H. Rojas, C. Granger, *Med. Devices: Evidence Res.* **2015**, *8*, 473.
[63] A. D. Augst, H. J. Kong, D. J. Mooney, *Macromol. Biosci.* **2006**, *6*, 623.
[64] H. A. Barnes, *J. Non-Newtonian Fluid Mech.* **1999**, *81*, 133.
[65] C. J. Pipe, T. S. Majmudar, G. H. McKinley, *Rheol. Acta* **2008**, *47*, 621.
[66] A. Malkin, V. Kulichikhin, S. Ilyin, *Rheol. Acta* **2017**, *56*, 177.
[67] A. Tripathi, K. C. Tam, G. H. McKinley, *Macromolecules* **2006**, *39*, 1981.
[68] H. Goldansaz, C.-A. Fustin, M. Wübbenhorst, E. van Ruymbeke, *Macromolecules* **2016**, *49*, 1890.
[69] C. S. O'Bryan, C. P. Kabb, B. S. Sumerlin, T. E. Angelini, *ACS Appl. Bio Mater.* **2019**, *2*, 1509.
[70] C. S. Y. Tan, G. Agmon, J. Liu, D. Hoogland, E.-R. Janeček, E. A. Appel, O. A. Scherman, *Polym. Chem.* **2017**, *8*, 5336.
[71] R. G. Larson, *The Structure and Rheology of Complex Fluids*, Oxford University Press, New York **1999**.
[72] A. Sheikhzadeh, J. Yoon, D. Formosa, B. Domanska, D. Morgan, M. Schiff, *Appl. Ergon.* **2012**, *43*, 368.

© 2020 Wiley-VCH GmbH